Silicon integrated multi-mode ring resonator

Ye, Mengyuan; Sun, Chunlei; Yu, Yu; Ding, Yunhong; Zhang, Xinliang

Published in:
Nanophotonics

Link to article, DOI:
10.1515/nanoph-2020-0556

Publication date:
2021

Document Version
Publisher's PDF, also known as Version of record

Research article

Mengyuan Ye, Chunlei Sun, Yu Yu*, Yunhong Ding and Xinliang Zhang

Silicon integrated multi-mode ring resonator

https://doi.org/10.1515/nanoph-2020-0556
Received October 3, 2020; accepted December 24, 2020;
published online January 18, 2021

Abstract: Ring resonator is an essential element in silicon integrated circuit, it is widely used as filter, wavelength multiplexer and switch in single-mode operation regime. As the rapid development of mode division multiplexing (MDM) technique, ring resonator that can process multi-mode signals simultaneously and uniformly is highly desired. However, the severe modal dispersion makes identical transmission for different modes very hard. In this paper, by breaking through the limitation of conventional multi-mode manipulation design with evanescent coupling or mode interference, we propose and demonstrate a multi-mode ring resonator (MMRR) inspired by the free space geometric optics. Arbitrary number of supporting modes can be achieved by simply widening the waveguide width. For proof-of-concept demonstration, an MMRR supporting four modes is fabricated with uniform transmittance. Furthermore, architecture of cascaded four MMRRs are also demonstrated experimentally.

Keywords: geometrical optics; integrated optics devices; multi-mode; ring resonator.

1 Introduction

Silicon photonics is commonly regarded as a promising solution for inter/intra data-centre connections due to its advantages as low-cost, strong mode confinement and compatibility with matured Complementary Metal-Oxide-Semiconductor (CMOS) technologies [1–3]. To meet the increasing demand of the chip-level transmission capacity, conventional multiplexing technologies on wavelength, polarization dimensions have been intensively utilized [4]. In the past decade, the mode division multiplexing (MDM) technique attracts more and more attentions by introducing high-order modes to further enlarge the transmission capacity [5]. To build up a chip-level MDM network, building blocks such as mode converter and mode multiplexer are exclusively investigated [6–12]. Other multi-mode processing elements including crossing and bend are also reported [13–17]. Furthermore, advanced circuits like multi-mode switches have also been demonstrated [18–22]. Multi-mode devices are playing key roles in MDM network.

Due to the severe modal dispersion in conventional silicon multi-mode waveguide, a demultiplexing-processing-multiplexing architecture is commonly utilized in multi-mode circuit, resulting in a complex and inefficient device layout. To address this problem, a novel mode insensitive architecture is introduced to process the MDM signals simultaneously, and a great deal of effort has been made [23–26], achieving the small-footprint and low-loss multi-mode power splitter, filter and switch.

Ring resonator, an essential element widely used in single-mode operation network [27], is highly desired in MDM system to realize significant applications like filtering, wavelength multiplexing and switching. However, it is not easy to realize a mode insensitive multi-mode ring resonator (MMRR), due to the severe modal dispersion existed in the coupling region and the bend waveguide. Reported MMRR [23] used adiabatic Bezier curve for 90° bend and optimized racetrack for uniform dual-mode coupling. This design method is time-consuming and hard to support more modes. Consequently, the demonstrated device only worked for two modes. Furthermore, severe difference on free spectral ranges (FSRs) for the two modes limits its application in practical system.

Mengyuan Ye and Chunlei Sun have contributed equally to this work.

***Corresponding author: Yu Yu**, Wuhan National Laboratory for Optoelectronics and School of Optical and Electrical Information, Huazhong University of Science and Technology, Wuhan 430074, China, E-mail: yuyu@mail.hust.edu.cn. https://orcid.org/0000-0002-8421-6794
Mengyuan Ye, Wuhan National Laboratory for Optoelectronics and School of Optical and Electrical Information, Huazhong University of Science and Technology, Wuhan 430074, China; and School of Automation, China University of Geosciences, Wuhan 430074, China
Chunlei Sun and Xinliang Zhang, Wuhan National Laboratory for Optoelectronics and School of Optical and Electrical Information, Huazhong University of Science and Technology, Wuhan 430074, China
Yunhong Ding, Department of Photonics Engineering, Technical University of Denmark, Building 343, 2800 Kgs. Lyngby, Denmark

In this paper, we break through the limitation of conventional multi-mode manipulation design thoughts such as evanescent coupling and mode interference. Inspired by free space geometric optics, we propose an MMRR with the help of total internal reflection (TIR) effect and frustrated TIR (FTIR) coupling method. The TIR and FTIR have been studied for free space optics [28]. In recent years, integrated devices based on TIR and FTIR structures become more and more attractive. Compact bend waveguide and coupler with broad bandwidth are demonstrated on thick silicon platform [29, 30]. Here, we introduce TIR and FTIR into the multi-mode ring resonator design, achieving the mode insensitive operation on 220 nm silicon-on-isolator (SOI) platform. By utilizing a wider waveguide, light propagates in the plane as in free space while still being confined vertically in the waveguide. In this case, the waveguide effect tends to be negligible in the plane, and thus light propagation can be considered as the ray trajectory in the media. Therefore, the modal dispersion issue that limits the conventional multi-mode manipulation is solved fundamentally. Arbitrary number of supporting modes can be achieved by simply widening the waveguide width. For demonstration, we design and fabricate the MMRR supporting four modes. Measured transmission spectra are in accordance with the simulation. High uniformities on FSR, insertion loss and crosstalk indicate that the proposed mode insensitive manipulation is successfully achieved. Furthermore, architecture of four cascaded MMRRs is demonstrated and characterized experimentally.

2 Design and simulation

Schematic diagram of the proposed MMRR is shown in Figure 1(a). The device consists of four 90° bends and two coupling regions, forming the ring loop and loop access, respectively. Different modes at resonance wavelengths are coupled into the ring through the In port, and coupled out from the Drop port. The effective indices for seven transverse electric (TE) modes with different waveguide widths are calculated and shown in Figure 1(b). It can be seen that the modal dispersion decreases with the waveguide width increasing. All modes tend to degenerate to the slab mode that propagates in the plane as in free space when waveguide width is much larger than the operation wavelength. Thus, different modes behave similar and a uniform process can be expected for all modes. Design and corresponding simulation details of the coupling region and 90° bends are introduced in following sections. The finite-difference time-domain (FDTD) method is utilized for the simulations of coupling region and 90° bends.

2.1 Coupling region

In order to realize uniform coupling for all modes, the coupling region needs to be specifically designed. The conventional coupling schemes rely on the theories of evanescent coupling and mode interference, such as the directional couplers (DCs) [24], multi-mode interference (MMI) couplers [26] and adiabatic couplers (ACs) [23]. Due to the severe modal dispersion, the interference image positions and coupling lengths differ significantly for different modes, making the coupling characters very different.

In free space geometric optics, cube beam splitter consisting of a pair of right-angle prisms is generally utilized for light splitting. Specific splitting ratio can be achieved by designing the metallic-dielectric coating between the two prisms. Here, we use the same concept to realize an on-chip multi-mode coupler. Figure 2(a) illustrates the schematic of the proposed multi-mode coupler. Two TIR mirrors are placed closely with a trench aligned 45° to the waveguide, forming a FTIR coupler [28, 29]. The TIR mirror and the trench correspond to right-angle prism and

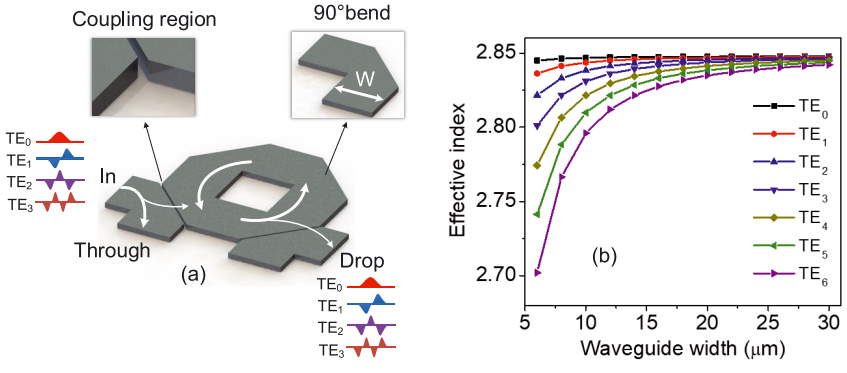

Figure 1: (a) Schematics of the multi-mode ring resonator. (b) Calculated effective indices for TE_0–TE_6 modes with different waveguide widths at 1550 nm.

metallic-dielectric coating, respectively. At the interface of TIR mirror, the light propagation field will decay exponentially and extend into the trench perpendicularly. Optical power will pass the trench and transmit into the Through port partially, while the rest power will be reflected to the Cross port at the interface. Thus, the coupling ratio can be controlled by selecting appropriate trench width *G*.

To realize sufficient coupling into the MMRR, coupling ratio for the TE_0–TE_3 modes with different trench widths are calculated and shown in Figure 2(b). Light is lunched into the In port, then monitored at the Cross port and Through port. In the legend "0-T", "0" stands for TE_0 mode, while the letter "T" refers to the Through port. To obtain a coupling ratio of 1:9, the trench width G is chosen to be 215 nm. Thus, the corresponding coupling efficiencies for TE_0–TE_3 modes are 0.3348, 0.3391, 0.3444 and 0.3521, respectively. The coupling efficiency of the FTIR coupler is dependent on the trench gap and depth. For our MMRR design, the designed coupling efficiency of ~10% is enough to obtain appropriate bandwidth and extinction ratio. By engineering the gap or shallow etching structure, different coupling ratio could be achieved. Please note that the slight difference among all modes is caused by the pinhole diffraction, which introduces the mode-dependent loss. The light propagations for TE_0 and TE_3 modes are shown in Figure 2(c) and (d), representing the lowest and highest order modes that to be demonstrated. The transmission spectra from 1500 to 1600 nm for TE_0 and TE_3 modes are also calculated, as shown in Figure 2(e) and (f). In the legend "01-T" and "01-C", "0" stands for the input TE_0 mode, while "1" stands for the output TE_1 mode. The letter "T" refers to the Through port, and the letter "C" refers to the Cross port. Insertion losses are simulated to be 0.02, 0.07, 0.18 and 0.32 dB for TE_0–TE_3 modes, respectively. The mode crosstalks for all modes are lower than –23 dB. High uniformities in teams of coupling ratio and insertion loss for all modes ranging from 1500 to 1600 nm can be observed, indicating excellent performance of the proposed structure.

2.2 90° bend

Being different from the arc-shaped waveguide utilized in conventional single-mode ring resonator, specific bend is required to support multi-mode transmission identically, and this is challenging due to the severe mode crosstalk. Conventional method is to engineer the mode effective indices for adiabatic transmission in bend waveguide [14]. However, the design of such a structure is complex and time consuming, which makes supporting more modes extremely hard.

To change propagation direction of light in free space geometric optics, a mirror is generally used. Here, we could

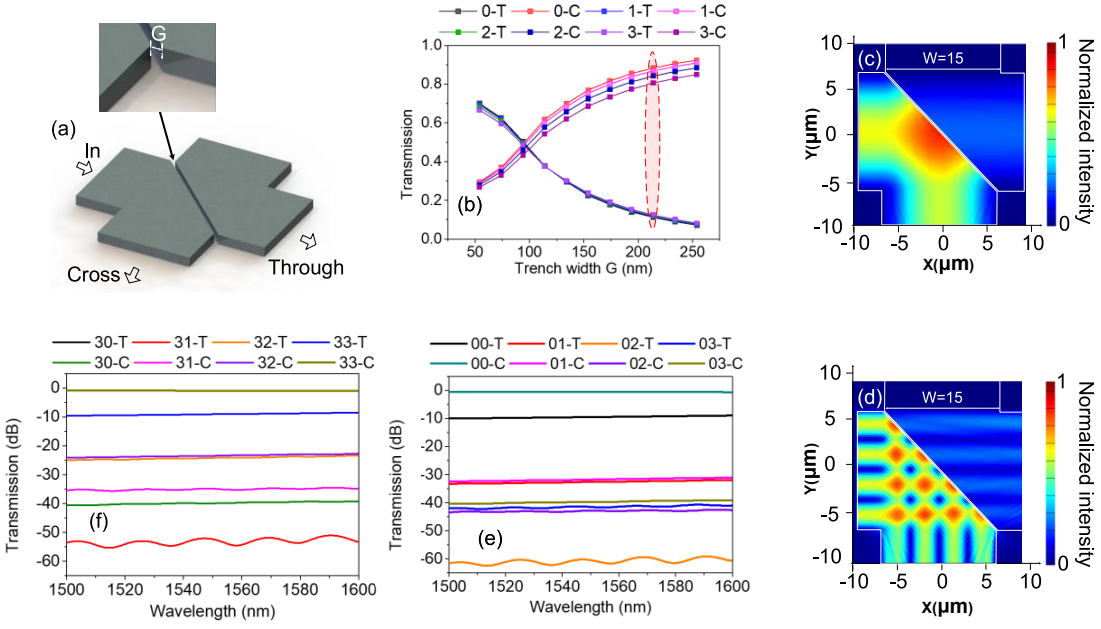

Figure 2: (a) Structure of the coupling region. (b) Simulated transmission efficiency for TE_0–TE_3 modes with different trench gaps. Simulated light propagations for (c) TE_0 and (d) TE_3 mode input and corresponding transmission spectra for (e) TE_0 and (f) TE_3 mode input from 1500 to 1600 nm.

also design the 90° bend by utilizing a waveguide-based TIR mirror. Figure 3(a) illustrates the schematic of our proposed multi-mode 90° bend on SOI waveguide. Critical angle θc of TIR for TE_0–TE_3 modes at 1550 nm are calculated and shown in Figure 3(b). For the bus waveguide with $W = 15\,\mu m$, the critical angles for the four modes tend to be a uniform value of 30.5°. In order to form the ring loop, the incident angle θ is chosen to be 45°, which is far beyond the critical angle. Figure 3(c) and (d) shows the simulated light propagation in 90° bends for TE_0 and TE_3 at 1550 nm, respectively. The transmission spectra from 1500 to 1600 nm are also calculated, as shown in Figure 3(e). Results indicate insertion loss for TE_0–TE_3 modes are ~0.019, 0.067, 0.15 and 0.27 dB, respectively. Crosstalks for all modes are lower than –25 dB within the 100 nm wavelength range.

2.3 MMRR

Based on the two key elements discussed above, an MMRR can be formed. In order to characterize the MMRR, the drop port transmission spectra for TE_0–TE_3 modes within one FSR are simulated, as the solid lines illustrated in Figure 4. Additionally, in order to investigate the performance considering fabrication errors, we fabricate the reference multi-mode coupler and 90° bend. By extracting measured insertion losses of the reference devices, round-trip parameters are updated, and thus transmission spectra considering the fabrication errors are re-calculated. The insertion loss of the coupling region for TE_0–TE_3 modes are measured to be 1.2 1.4, 1.8 and 2.4 dB, respectively. While the insertion loss of the 90° bend for TE_0–TE_3 modes are measured to be 0.04 0.12, 0.21 and 0.52 dB, respectively. The updated transmission spectra considering fabrication errors are shown as the dash lines in Figure 4. In the legend "00-S" and "00-M", the first "0" stands for the input TE_0 mode, while the second "0" stands for the output TE_0 mode. "S" stands for the simulation without fabrication loss being taken into account, while "M" stands for the simulation with measured fabrication loss being considered. To be noted, the curves labelled "23-M" and "23-S" present the highest crosstalk among all instances.

For the circumstance without fabrication errors being included, the simulated results indicate insertion loss for TE_0–TE_3 modes are ~0.35, 1.1, 2.26 and 3.66 dB, respectively. Insertion loss is attributed to the round-trip light propagation. Thanks to a wilder waveguide structure utilized for the MMRR, propagation loss could be ignored. Insertion loss is mainly caused by the scattering at the TIR mirror surface. Taking Goos–Hänschen shift into consideration and utilizing optimized bend structure could reduce the interface scattering, and thus improve the insertion loss [30]. To be noted, the phase shift caused by

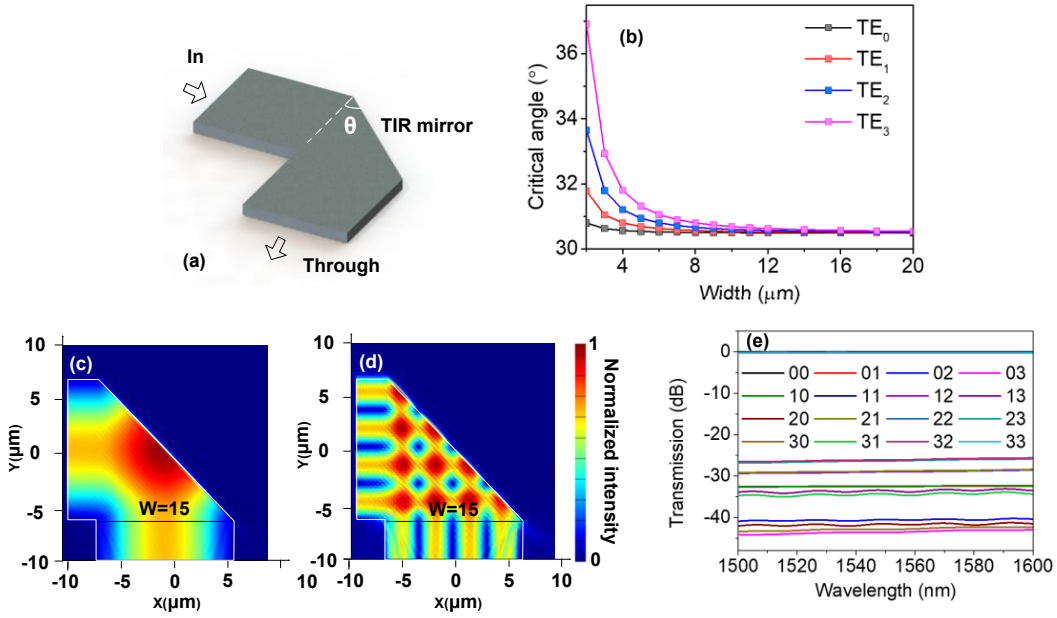

Figure 3: (a) Structure of the 90° bend with TIR. (b) Simulated critical angle for TE_0–TE_3 modes with different waveguide widths at 1550 nm. Simulated light propagations for (c) TE_0 and (d) TE_3 mode input and corresponding transmission spectra for (e) TE_0 and (f) TE_3 mode input from 1500 to 1600 nm. In the legend "01", "0" stands for the input TE_0 mode, while "1" stands for the output TE_1 mode.

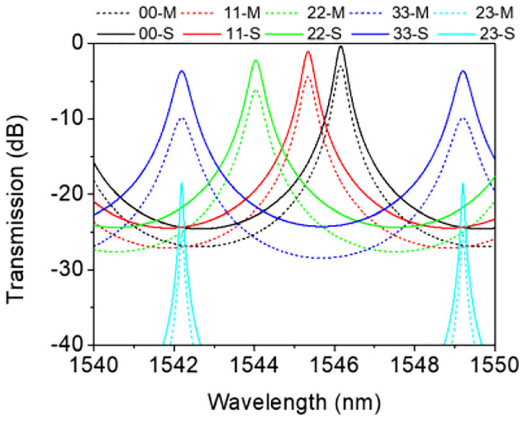

Figure 4: Simulated transmission spectra of the MMRR for TE_0–TE_3 mode input within one FSR with (dash lines) and without (solid lines) considering the fabrication loss.

the Goos–Hänschen shift will lead to slightly different FSRs for different modes. In our design, the Goos–Hänschen shift for mode TE_0 and TE_3 is 175.94 and 176.73 nm, leading to a difference of ~0.001 nm on FSRs. To reduce this difference, waveguide structure could be further optimized for lower modal dispersion, e.g. by utilizing wider or smaller index-contrast waveguide under the premise of TIR. Meanwhile, difference of insertion losses among all modes, i.e. the mode dependent loss, is mainly introduced by the pinhole diffraction, which could be alleviated by adopting a wider waveguide. Crosstalks for all modes are lower than –15 dB. Thanks to the similar effective indices for all modes, similar FSRs around 6.65 nm for all modes can be observed, indicating a good performance for the proposed MMRR. For the circumstance with fabrication loss being involved, insertion losses for TE_0–TE_3 modes are updated to be ~3, 4.46, 6.21 and 9.92 dB, respectively. To be noted, the additional loss is mainly caused by the fabrication errors of the trench, which can be reduced by optimizing the fabrication tolerance of the multi-mode coupling regions.

3 Fabrication

The proposed circuit is designed and fabricated based on the SOI wafer with top silicon layer of 220 nm and SiO_2 buried layer of 2 μm. The electron beam lithography (EBL) and inductively coupled plasma (ICP) etching are used to form the waveguide structure. A 1-μm thick SiO_2 cladding by plasma-enhanced chemical vapour deposition (PECVD) covers the entire device, forming a buffer layer between the heater and the waveguides. The metal Au electrode is sputtered on a separate layer, realizing the connection to the external electrical source with TiN heaters. The width of multimode waveguide is designed as 15 μm. To form the rib waveguide, full etching is adopted. And the trench gap of the coupling region is chosen to be 215 nm. In order to tune the resonant wavelength of MMRR, an integrated Ti heater is fabricated on top of the MMRR. The thickness and the width of the heaters are 130 nm and 4 μm, respectively. The heating efficiency is measured to be 35 mW/FSR. The narrower heater leads to the uneven heat distribution for different modes, and thus the resonance wavelength tuning for each mode will be different. Optimization on heater structure could be further performed to mitigate this issue. The grating couplers (GCs) are used to couple light into and out of the chip. Adiabatic linear tapers with a length of 600 μm are fabricated to connect the mode mux/demux and MMRR. It can be significantly shortened by utilizing specific design [31]. The layout of the fabricated MMRR is illustrated in Figure 5(a) and the zoomed-in view is shown in Figure 5(b). Footprint of the fabricated MMRR is 40 μm × 40 μm. Four cascaded MMRRs are also fabricated, the microscope image is shown in Figure 5(c). In order to test the proposed MMRR, mode multiplexer and demultiplexer are adopted for TE_0–TE_3 mode excitation. The mode (de)multiplexer utilized is formed by cascaded couplers, and the operation principle is based on the adiabatic mode evolution with two counter tapered waveguide [32]. The insertion losses for TE_0–TE_3 modes are measured to be ~0.7, 0.7, 1.4 and 1.8 dB, respectively, and the mode crosstalk is ~–12 dB in the wavelength range of 1520–1560 nm.

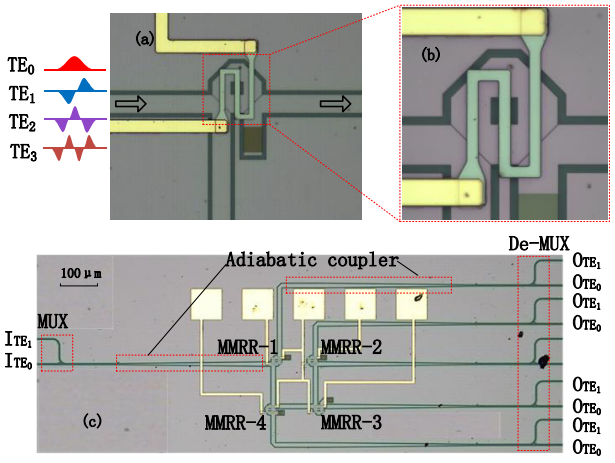

Figure 5: (a) Microscope image of the fabricated MMRR. (b) Zoom-in view. (c) Image of the fabricated cascaded MMRRs.

4 Measurement and results

Broadband light source from 1530 to 1590 nm is launched into the circuit. Assisted by the polarization beam splitter and polarization controller, the linearly polarized input can be achieved. A power meter is utilized to monitor the output light while an optical spectrum analyser (OSA) is used to measure the transmission spectra. Both single MMRR and cascaded MMRRs are measured. Details of the measured results are demonstrated and discussed in the following sections.

4.1 MMRR for four modes

In order to verify the performance of the fabricated MMRR, transmission spectra from 1530 to 1590 nm for signals injection with different modes are measured and shown in Figure 6(a). To illustrate the results clearly, spectra within one FSR are also demonstrated, as shown in Figure 6(b). The spectra of different modes are intentionally detuned for a better comparison.

The insertion losses for TE_0–TE_3 mode are measured to be 4.85, 7.18, 11.5 and 11 dB, respectively. FSRs for TE_0–TE_3 mode are measured to be 6.4, 6.36, 6.41 and 6.35 nm. The quality factors (Q-factors) for TE_0–TE_3 modes are measured to be ~7300, 5700, 4500 and 4800, respectively. Since the Q factor is dependent to the round-trip loss and coupling efficiency of the coupler, the low-loss bends and appropriate coupling gap could reduce the reflection and scattering loss efficiently, achieving a high Q factor. Extinction ratio of more than 20 dB can be observed for all four modes. Mode crosstalks for TE_0–TE_3 mode output are measured to be –12, –8, –7 and –10 dB, respectively. Results of insertion loss and FSR accord well with the simulation. FSRs with high uniformity for all modes indicate that the mode insensitive manipulation is successfully achieved. To be noted, the measured crosstalk is larger than the simulated value, and this is caused by the poor performance of the mode multiplexer used in the scheme (–12 dB crosstalk). By adopting better mode multiplexer, performance on crosstalk could be improved.

4.2 Cascaded MMRRs

Being commonly utilized as filters, modulators and WDM demultiplexers [33, 34], cascaded ring resonators is regarded as an important architecture in single-mode regime. In order to achieve those important functionalities in multi-mode regime, we further demonstrate the architecture of four cascaded MMRRs experimentally. With the help of on-chip mode mux/de-mux and adiabatic couplers, signals with TE_0 and TE_1 mode are lunched into the cascaded MMRRs from the input port and detected at the corresponding output ports, as shown in Figure 5(c). The transmission spectra for four MMRRs from 1540 to 1560 nm are measured and shown in Figure 7. In the legend "00-1", "00" stands for the TE_0 mode input and output, while "1" stands for the number of MMRR labelled in Figure 5(c). Remarkable high uniformities for different MMRRs in terms of FSR, extinction ratio and bandwidth can be observed from the measured spectra, indicating a good potential for multi-mode signal processing. The demonstrated cascaded architecture can be further utilized in advanced WDM–MDM transmission system.

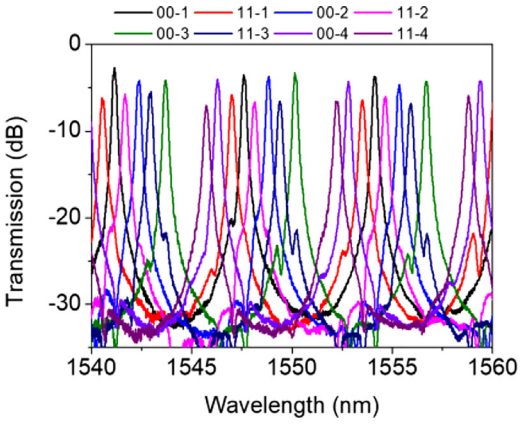

Figure 7: Measured transmission spectra of the cascaded four MMRRs for TE_0 and TE_1 mode input from 1540 to 1560 nm.

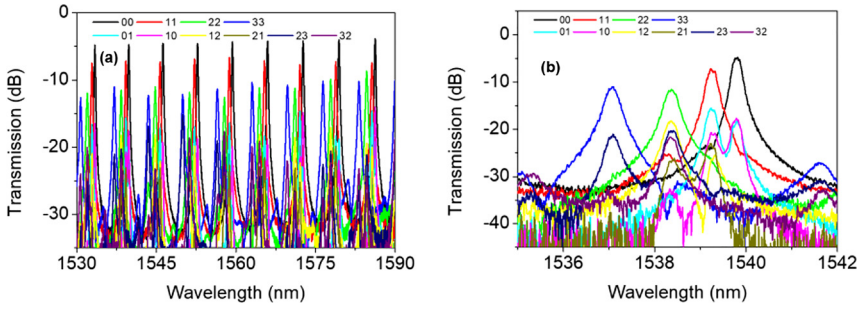

Figure 6: Measured transmission spectra of the MMRR for TE_0–TE_3 mode input (a) from 1530 to 1590 nm and (b) within one FSR.

5 Conclusion

In summary, we propose and demonstrate a silicon integrated multi-mode ring resonator. In analogy with the free space geometric optics design, arbitrary number of supporting modes can be achieved by simply widening the waveguide width. The MMRR supporting four modes is fabricated as a proof-of-concept demonstration. Measured transmission spectra are in accordance with the simulation. High uniformities on FSR, insertion loss and crosstalk indicate that the proposed mode insensitive manipulation is successfully achieved. Furthermore, cascaded architecture of four MMRRs is demonstrated experimentally. Measured transmission spectra indicate the good potential for multi-mode signal processing.

Author contributions: All the authors have accepted responsibility for the entire content of this submitted manuscript and approved submission.
Research funding: This work was supported by the National Key Research and Development Program of China (2019YFB1803801, 2019YFB2203502), National Natural Science Foundation of China (61922034, 61911530161), Program for HUST Academic Frontier Youth Team (2018QYTD08).
Conflict of interest statement: The authors declare no conflicts of interest.

References

[1] L. Chrostowski and M. Hochberg, *Silicon Photonics Design: From Devices to Systems*, Cambridge, UK, Cambridge University Press, 2015.
[2] R. Soref, "The past, present, and future of silicon photonics," *IEEE J. Sel. Top. Quant. Electron.*, vol. 12, pp. 1678–1687, 2006.
[3] C. Sun, M. T. Wade, Y. Lee, et al., "Single-chip microprocessor that communicates directly using light," *Nature*, vol. 528, pp. 534–538, 2015.
[4] C. Doerr and T. Taunay, "Silicon photonics core-, wavelength-, and polarization-diversity receiver," *IEEE Photonics Technol. Lett.*, vol. 23, pp. 597–599, 2011.
[5] P. J. Winzer, "Making spatial multiplexing a reality," *Nat. Photonics*, vol. 8, pp. 345–348, 2014.
[6] D. Dai, J. Wang, and Y. Shi, "Silicon mode (de)multiplexer enabling high capacity photonic networks-on-chip with a single-wavelength-carrier light," *Opt. Lett.*, vol. 38, pp. 1422–1424, 2013.
[7] J. Wang, P. Chen, S. Chen, Y. Shi, and D. Dai, "Improved 8-channel silicon mode demultiplexer with grating polarizers," *Opt. Express*, vol. 22, pp. 12799–12807, 2014.
[8] J. B. Driscoll, R. R. Grote, B. Souhan, J. I. Dadap, M. Lu, and R. M. Osgood, "Asymmetric Y junctions in silicon waveguides for on-chip mode-division multiplexing," *Opt. Lett.*, vol. 38, pp. 1854–1856, 2013.
[9] D. Chen, X. Xiao, L. Wang, Y. Yu, W. Liu, and Q. Yang, "Low-loss and fabrication tolerant silicon mode-order converters based on novel compact tapers," *Opt. Express*, vol. 23, pp. 11152–11159, 2015.
[10] J. Leuthold, J. Eckner, E. Gamper, P. A. Besse, and H. Melchior, "Multimode interference couplers for the conversion and combining of zero-and first-order modes," *J. Lightwave Technol.*, vol. 16, p. 1228, 1998.
[11] L.-W. Luo, N. Ophir, C. P. Chen, et al., "WDM-compatible mode-division multiplexing on a silicon chip," *Nat. Commun.*, vol. 5, p. 3069, 2014.
[12] C. Sun, Y. Yu, M. Ye, G. Chen, and X. Zhang, "An ultra-low crosstalk and broadband two-mode (de) multiplexer based on adiabatic couplers," *Sci. Rep.*, vol. 6, p. 38494, 2016.
[13] H. Xu and Y. Shi, "Dual-mode waveguide crossing utilizing taper-assisted multimode-interference couplers," *Opt. Lett.*, vol. 41, pp. 5381–5384, 2016.
[14] L. H. Gabrielli, D. Liu, S. G. Johnson, and M. Lipson, "On-chip transformation optics for multimode waveguide bends," *Nat. Commun.*, vol. 3, pp. 1–6, 2012.
[15] Y. Wang and D. Dai, "Multimode silicon photonic waveguide corner-bend," *Opt. Express*, vol. 28, pp. 9062–9071, 2020.
[16] C. Sun, Y. Yu, and X. Zhang, "Ultra-compact waveguide crossing for a mode-division multiplexing optical network," *Opt. Lett.*, vol. 42, pp. 4913–4916, 2017.
[17] C. Sun, Y. Yu, G. Chen, and X. Zhang, "Ultra-compact bent multimode silicon waveguide with ultralow inter-mode crosstalk," *Opt. Lett.*, vol. 42, pp. 3004–3007, 2017.
[18] B. Stern, X. Zhu, C. P. Chen, et al., "On-chip mode-division multiplexing switch," *Optica*, vol. 2, pp. 530–535, 2015.
[19] C. Sun, Y. Yu, G. Chen, and X. Zhang, "On-chip switch for reconfigurable mode-multiplexing optical network," *Opt. Express*, vol. 24, pp. 21722–21728, 2016.
[20] L. Yang, T. Zhou, H. Jia, et al., "General architectures for on-chip optical space and mode switching," *Optica*, vol. 5, pp. 180–187, 2018.
[21] Y. Zhang, Y. He, Q. Zhu, C. Qiu, and Y. Su, "On-chip silicon photonic 2×2 mode-and polarization-selective switch with low inter-modal crosstalk," *Photonics Res.*, vol. 5, pp. 521–526, 2017.
[22] C. Sun, W. Wu, Y. Yu, et al., "De-multiplexing free on-chip low-loss multimode switch enabling reconfigurable inter-mode and inter-path routing," *Nanophotonics*, vol. 7, pp. 1571–1580, 2018.
[23] B. A. Dorin and N. Y. Winnie, "Two-mode division multiplexing in a silicon-on-insulator ring resonator," *Opt. Express*, vol. 22, pp. 4547–4558, 2014.
[24] Y. Luo, Y. Yu, M. Ye, C. Sun, and X. Zhang, "Integrated dual-mode 3 dB power coupler based on tapered directional coupler," *Sci. Rep.*, vol. 6, p. 23516, 2016.
[25] K. Chen, J. Yan, S. He, and L. Liu, "Broadband optical switch for multiple spatial modes based on a silicon densely packed waveguide array," *Opt. Lett.*, vol. 44, pp. 907–910, 2019.
[26] G. Zhang, H. R. Mojaver, A. Das, and O. Liboiron-Ladouceur, "Mode insensitive switch for on-chip interconnect mode division multiplexing systems," *Opt. Lett.*, vol. 45, pp. 811–814, 2020.
[27] W. Bogaerts, P. De Heyn, T. Van Vaerenbergh, et al., "Silicon microring resonators," *Laser Photonics Rev.*, vol. 6, pp. 47–73, 2012.
[28] S. Zhu, A. Yu, D. Hawley, and R. Roy, "Frustrated total internal reflection: a demonstration and review," *Am. J. Phys.*, vol. 54, pp. 601–607, 1986.

[29] N. R. Huntoon, M. P. Christensen, D. L. MacFarlane, G. A. Evans, and C. Yeh, "Integrated photonic coupler based on frustrated total internal reflection," *Appl. Opt.*, vol. 47, pp. 5682–5690, 2008.

[30] T. Aalto, M. Harjanne, S. Ylinen, M. Kapulainen, T. Vehmas, and M. Cherchi, *Total Internal Reflection Mirrors with Ultra-Low Losses in 3 μm Thick SOI Waveguides*, vol. 9367, San Francisco, California, USA, SPIE OPTOSPIE, 2015. Available at: https://doi.org/10.1117/12.2079748.

[31] W. Qi, Y. Yu, and X. Zhang, "On-chip arbitrary-mode spot size conversion," *Nanophotonics*, vol. 9, pp. 4365–4372, 2020.

[32] J. Wang, Y. Xuan, M. Qi, et al., "Broadband and fabrication-tolerant on-chip scalable mode-division multiplexing based on mode-evolution counter-tapered couplers," *Opt. Lett.*, vol. 40, pp. 1956–1959, 2015.

[33] Q. Xu, B. Schmidt, J. Shakya, and M. Lipson, "Cascaded silicon micro-ring modulators for WDM optical interconnection," *Opt. Express*, vol. 14, pp. 9431–9436, 2006.

[34] A. Gazman, C. Browning, Z. Zhu, L. R. Barry, and K. Bergman, "Automated thermal stabilization of cascaded silicon photonic ring resonators for reconfigurable WDM applications," in *2017 European Conference on Optical Communication (ECOC)*, IEEE, 2017, pp. 1–3.